

Primary Side Control Based Inductively Coupled Powering Scheme for Biomedical Implants

Manzil Zaheer, *Student Member, IEEE*, Jaspreet Singh Suri, and Harshal B Nemade, *Member, IEEE*

Abstract—This paper proposes a novel and easy technique to implement primary control for inductively coupled power transfer systems. With the proposed design, the control law boils down simply to a multiplication of voltages across two capacitors in the primary side. The advantages include easy implementation and the topology is favourable for biomedical application, as any chance of heating due to presence of power flow controller in secondary side is eliminated. The effectiveness of the proposed power pickup and its applicability to general wireless power transfer applications has been demonstrated by both simulation and experimental results.

I. INTRODUCTION

INDUCTIVELY coupled power transfer (ICPT) systems are designed to deliver power efficiently from a stationary primary source to one or more movable secondary loads over relatively large gaps via magnetic coupling. It is based on the fundamental principles of electromagnetism discovered by Ampere and Faraday that make use of alternating magnetic fields around current carrying conductors to transfer power from a primary winding to a secondary winding.

The advancement of power electronics has led to the development of contactless powering schemes which can be of great use in mobile phones [1], biomedical implants [2], and battery charging for electrical vehicles [3] as well as other compact electronic devices [4]. The major driving force behind the development of contactless powering schemes is the added benefits in terms of safety, reliability, low maintenance costs and long product life.

The mutual coupling of ICPT systems is generally weak, thus to deliver the required power and ensure manageable equipment size, it is necessary to operate at high frequency. In addition, resonant circuits are normally employed in the primary and/or secondary networks to boost the power transfer capability, while minimizing the required VA rating of the power supply. For a general ICPT system topology as shown in Figure 1, there are three prime locations for controlling power flow – primary side control [2], [5] pickup control [6], [7] and post rectification control [1], [8].

This paper is organized as: Section II describes the major

Manzil Zaheer is an undergraduate student at the Electronics and Electrical Engineering Department, Indian Institute of Technology Guwahati, India. (phone: +91-9435599522; e-mail: manzil@iitg.ac.in).

Jaspreet Singh Suri is an undergraduate student at the Electronics and Electrical Engineering Department, Indian Institute of Technology Guwahati, India. (e-mail: s.jaspreet@iitg.ac.in).

Harshal.B.Nemade is an Associate Professor at the Electronics and Electrical Engineering Department, Indian Institute of Technology Guwahati, India. (e-mail: harshal@iitg.ac.in).

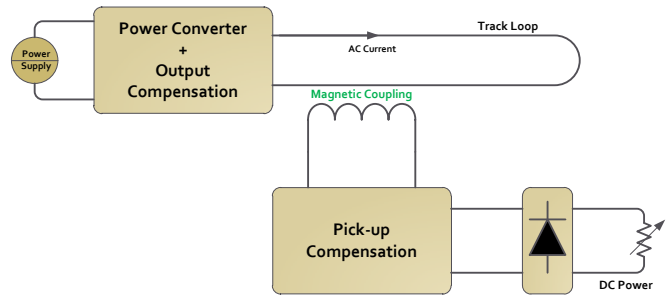


Figure 1: General topology of ICPT system

challenges and short-comings of presently available powering schemes for biomedical implantable devices; Section III, IV and V deal with proposed solutions for the problems described in II; finally Section VI presents the simulation result followed by experimental verification and paper concludes with Section VII.

II. MAJOR CHALLENGES

In biomedical implants the power requirements are increasing [9]. Use of transcutaneous electrodes cause discomfort to the patient and imposes the risk of infection, thus compromising quality of life. Use of internal batteries limits the life of implants and involves invasive methods like surgery for replacement. Inductive power transfer schemes have been proposed for the purpose as a solution. But, maintaining an uninterrupted inductive power link to the vital implants maybe difficult for the patient in day-to-day life. Therefore, a new resolution combining the above mentioned methods is proposed which adopts a high performance rechargeable battery with periodic charging through ICPT system. The rechargeable battery can provide stable and clean supply voltage independently, and the life span of the implants will be extended substantially.

While designing any biomedical implants, an important criterion is that the device should not be heated by more than 2 °C above the body temperature [10], [11]; else it might harm surrounding living tissues. Additionally magnetic field intensity and frequency of the inductive power link must be kept within the safety limits. Thus the authors propose an inductive power link with a simple secondary pickup and controller on primary side with an attempt to dissipate most of the losses at the primary side i.e. outside the body.

III. PROPOSED ARCHITECTURE

Figure 2 shows the proposed ICPT system with only one controller, employed on primary side. A resonant circuit is used to generate the track current at the desired frequency,

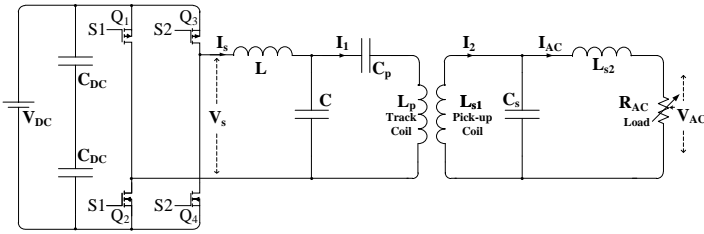


Figure 2: Proposed ICPT system

which can range from 10-1000 kHz. The primary side controller drives the inverter in such a way so as to maintain a desired amount of current in the primary winding, which is referred to as the track current, compensating for any variations in input supply and pick-up load. For ICPT systems with multiple pickups, a constant track current is essential but for the said application a varying track current maybe employed, as it is limited to a single pick-up. The mobile pickup unit comprises of an inductor-capacitor-inductor (T-LCL) resonant circuit, tuned to the same track frequency, in order to provide compensation and maximize the amount of power delivery. For system level analysis and control strategy evaluation rectifier and actual DC load is lumped as an equivalent AC resistance.

A. Inverting Circuit

The output voltage of a voltage-fed inverting network is completely governed by the switching devices of the inverting network. As a consequence, the track current can be regulated by duty cycle control of the switching pulses. One control strategy is to shift the phase of gate signals. In Figure 2, the switches Q_1 and Q_2 , Q_3 and Q_4 are controlled by the same gate signals S1 and S2 if PMOS – NMOS pair is used in each of the bridge arms, whereas they are complementarily controlled for total NMOS inverter. If both the upper switches Q_1 and Q_3 (or both the lower switches Q_2 and Q_4) are “on”, the AC output voltage from the inverting network is zero. Otherwise, the output voltage will be either positive V_{DC} or negative V_{DC} , depending on the state of the switches. Because of this, phase-shift duty cycle control can be utilised to regulate the output voltage and consequently the track current. Figure 3 shows a situation when the gate signals of Q_3 and Q_4 are lagging Q_1 and Q_2 by 90° . In this case, the output voltage is a PWM square wave with a duty cycle of $2/4$ (50%). It is obvious that if Q_1 (Q_2) and Q_3 (Q_4) are completely in phase, i.e. the phase shift is zero; the output voltage will be zero. On the other hand, if the switching is completely out of the phase, i.e. the phase shift is 180 degrees, then the output voltage reaches its maximum value with a fundamental magnitude (rms) given by:

$$V_s = \frac{4}{\pi\sqrt{2}} V_{DC} \quad (1)$$

In a more general case where the phase shift angle ψ is between zero degrees and 180 degrees, this voltage can be expressed as:

$$V_s = \frac{4}{\pi\sqrt{2}} V_{DC} \sin\left(\frac{\psi}{2}\right) \quad (2)$$

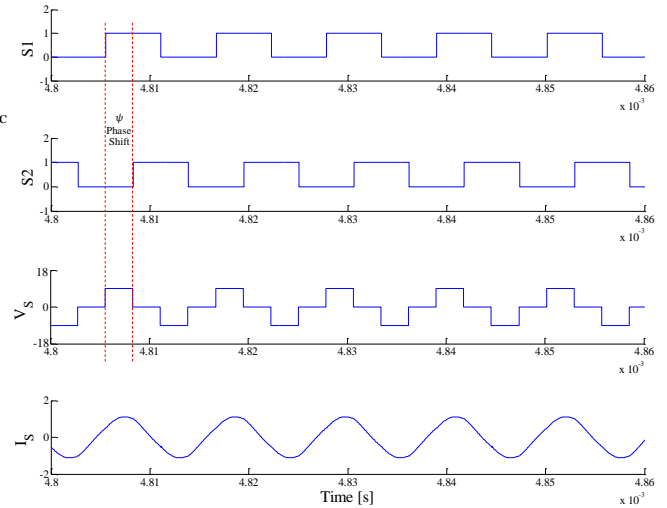


Figure 3: Phase shift control

B. Tuning Circuit Specifications

For tuning the circuit choose reactive components matched to the resonant frequency ω_0 as

- i. $\omega_0^2 LC = 1$
- ii. $\omega_0^2 L_p C_p = 1$
- iii. $\omega_0^2 (L_{S1} \parallel L_{S2}) C_s = 1$

Additionally $L = L_{S2}$, which are ready-made isolated inductors. The reason for which will be explained in section IV while designing the controller. Here the symbols represent passive elements as represented in Figure 2.

C. Primary Side

The primary side can be modelled as a tuning circuit driven by sinusoidal excitation as shown in Figure 4, with Z_r as the reflected load. Using Norton transformation the voltage source can be replaced by a current source. The inductor L and capacitor C come in parallel. If the circuit operates at the resonant frequency ω_0 , the parallel LC resonant circuit can be treated as open circuit and series $L_p C_p$ resonant circuit will behave as short circuit, resulting in constant current being fed to the reflected load which is given by:

$$I_1 = I_s = \frac{V_s}{j\omega L} \quad (3)$$

D. Secondary Side

The secondary side pickup circuit can be modelled as driven by a sinusoidal excitation with magnitude equal to open circuit voltage (V_{OC}) across the pickup coil as shown in

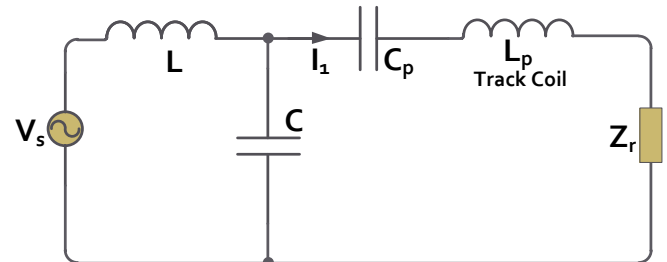


Figure 4: Modelled primary side

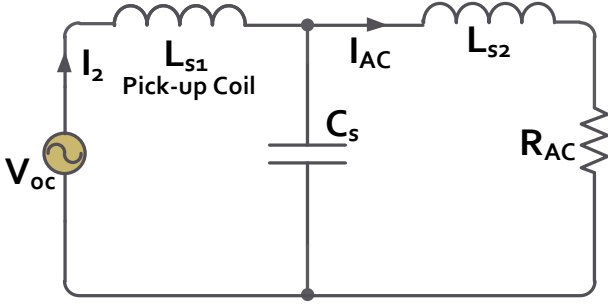


Figure 5: Modelled secondary side

Figure 5. Using Norton transformation the voltage source can be replaced by a current source. Notational splitting of the capacitor C_s into two capacitor C_{s1} and C_{s2} , i.e. $C_s = C_{s1} + C_{s2}$, such that they are tuned to L_{s1} and L_{s2} respectively, as shown in Figure 6. Observing that under fully tuned conditions, L_{s1} and C_{s1} which are in parallel will behave as open circuit. Applying Thevenin transformation, transforming the current source into a voltage source brings C_{s2} and L_{s2} in series which acts as a short circuit, under fully tuned conditions.

It can be seen from the above circuit simplification that the pickup acts as a voltage source to the load under fully tuned operation. Constant voltage can be maintained across the load if the induced open circuit voltage in the pickup coil can be maintained to be constant. This fact is exploited in the controller design as described in detail in section IV.

The pickup coil current I_2 is given by

$$I_2 = \frac{V_{oc}}{Z_s} \quad (4)$$

where Z_s is the total impedance of the secondary side circuit which is

$$Z_s = X_{L_{s1}} + X_{C_s} \parallel (X_{L_{s2}} + R_{AC})$$

Thus,

$$I_2 = \frac{L_{s2}}{L_{s1}} \left(\frac{L_{s2}}{L_{s1} R_{AC}} - j\omega C_s \right) V_{OC} \quad (5)$$

E. Induction

The primary side and secondary mobile pick-up is inductively coupled. The open circuit voltage induced in the secondary pick-up coil can be expressed in terms of mutual induction M between the primary and secondary coil and the primary track current as

$$V_{oc} = j\omega M I_1 \quad (6)$$

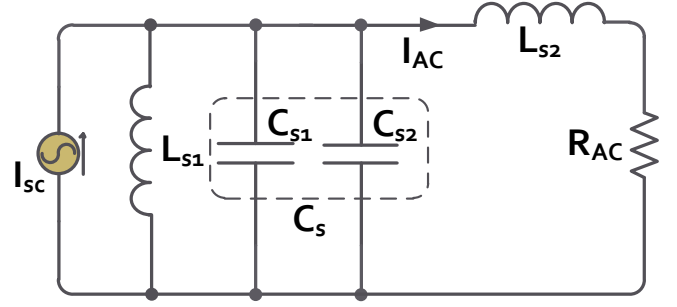


Figure 6: Abstract splitting of tuning capacitance

The reflected voltage on the primary side is

$$V_r = -j\omega I_2 = -\frac{\omega^2 M^2}{L_{s1}} \left(C_s + j \frac{L_{s2}}{\omega L_{s1} R_{AC}} \right) V_s \quad (7)$$

IV. CONTROLLER DESIGN

The controller objective would be to maintain a constant voltage across the load despite variations in the load or coupling between primary and secondary. As observed in the previous sections, voltage across the load depends on the open circuit voltage which in turn depends on the primary track current. Thus, to effectively maintain a constant voltage across the load in the secondary side, this voltage must be estimated at the primary side. Many controller designs have been proposed [2], [11], [12] and [13] which involve use of RF links or load modulation to convey this information (feedback) from secondary to primary. Either of the method increase circuit complexity at the secondary side, making the implant larger. In this work, the authors propose a very simple technique by which the voltage across the load at secondary can be estimated from the primary side tuning circuit itself, without any extra circuit in secondary side.

Basically there are two variables, namely M , the mutual induction between the primary and secondary and R_{AC} , the load itself, which need to be determined by the controller and accordingly assert control action to vary the primary track current appropriately. So controller topology as depicted in Figure 7 is proposed.

Notice that voltage across the load is boosted by a factor of L_{s2}/L_{s1} and given by

$$V_{AC} = \frac{L_{s2}}{L_{s1}} V_{oc} \quad (8)$$

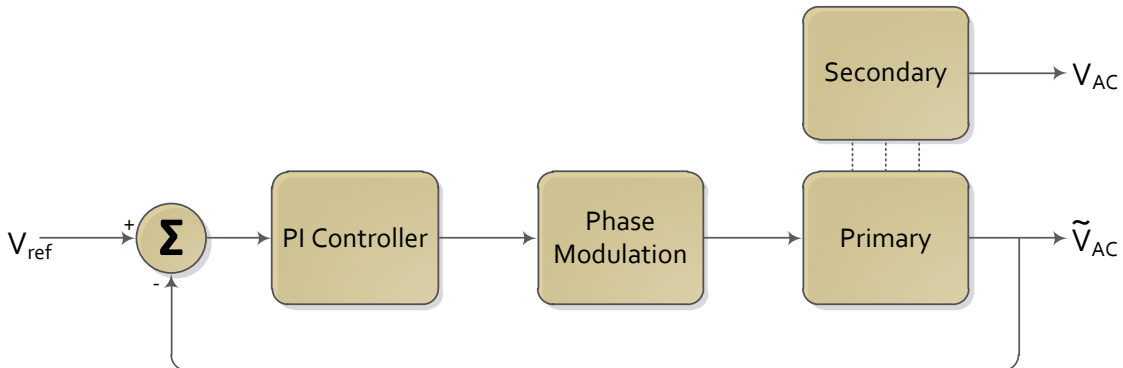


Figure 7: Controller topology

From (3) and (6)

$$V_{AC} = \frac{MV_s}{L_{s1}} \quad (9)$$

Mutual Inductance M can be estimated with help of (7)

$$\tilde{M} = \sqrt{\frac{-\Re\{V_r\}L_{s1}}{\omega^2 C_s V_s}} \quad (10)$$

Then voltage across the load can be estimated as

$$\tilde{V}_{AC} = \sqrt{\frac{-\Re\{V_r\}V_s}{\omega^2 C_s L_{s1}}} \quad (11)$$

From the tuning condition $\omega^2 = 1/L_{s1}C_{s1}$,

$$\tilde{V}_{AC} = \sqrt{-\frac{C_{s1}}{C_s} \Re\{V_r\}V_s} \quad (12)$$

In phasor form $\Re\{V_r\}$ implies $V_r \cos \phi$, where ϕ is the phase shift or the power factor, which implies

$$\tilde{V}_{AC} = \sqrt{-\frac{C_{s1}}{C_s} V_r V_s \cos \phi} \quad (13)$$

Practical implementation of the above control law is *quite simple*; in fact it is just the multiplication of voltages across two capacitors followed by low pass filtering.

Consider the capacitors C and C_p , let voltages across them be denoted by V_c and V_{cp} respectively then

$$\begin{aligned} V_c &= V_r \\ V_{cp} &= -\frac{V_s}{\omega^2 L C_p} \end{aligned} \quad (14)$$

under fully tuned conditions. Then substituting above relations in the control law results in

$$\tilde{V}_{AC} = \sqrt{\frac{C_{s1} C_p}{C_s C} V_c V_{cp} \cos \phi} \quad (15)$$

In time domain full expression of voltage across C and C_p would be

$$\begin{aligned} V_c(t) &= V_r(t) = V_c \cos(\omega t + \phi) \\ V_{cp}(t) &= V_{cp} \cos(\omega t) \end{aligned} \quad (16)$$

Consider

$$\begin{aligned} m(t) &= V_c(t)V_{cp}(t) \\ &= V_c V_{cp} \cos(\omega t + \phi) \cos(\omega t) \\ &= \frac{V_c V_p}{2} [\cos(\phi) + \cos(2\omega t + \phi)] \end{aligned} \quad (17)$$

upon elimination of the double frequency term by an LPF leaves only

$$r(t) = \frac{V_c V_{cp}}{2} \cos \phi \quad (18)$$

The signal $r(t)$ is easy to obtain and the control law can be expressed in terms of $r(t)$

$$\tilde{V}_{AC} = \sqrt{\alpha r(t)} \quad (19)$$

where α is a constant given by

$$\alpha = 2 \times \frac{C_{s1} C_p}{C_s C} \quad (20)$$

Realization of controller can be simplified further by ignoring the square root and providing V_{ref}^2 as the desired reference.

V. CURRENT PUMP BATTERY CHARGER

Traditional battery charging methods have low battery charging efficiency [14]. These methods apply constant current to the battery without allowing any resting period for the battery and thus causing a reduction in the charging efficiency and heat dissipation. Secondly, traditional methods do not provide any indication for the end of charging. Missing the end of charging time can also cause a reduction in the battery capacity and heat dissipation [15]. Therefore, current-pumped battery charger (CPBC) as proposed in [16] is used to increase the battery charging performance and as claimed raises tissue temperature no more than 2.1 °C [14].

The current pump battery charger consists of two main components: battery voltage monitor and charge-pumped phase-locked loop (CP-PLL), and also the reference oscillator f_{ref} corresponding to the nominal voltage of the battery. The operation of the current pump based battery charger (see Figure 8) is as follows: The battery voltage monitor converts the battery voltage to the VCO input range. The VCO frequency f_{vco} is compared with f_{ref} by the 3-state phase/frequency comparator (PFC) of the CP-PLL. Based on the difference between these two frequencies the frequency and the duty cycle of the pulse train from PFC are determined. At the beginning of the charging process when the battery voltage is quite low compared to its nominal voltage, the CP-PLL will be in frequency tracking mode and duty cycle will be 100% (i.e., DC) resulting in constant charging current (I_b). As the charging progresses, battery voltage increases and CP-PLL will lock into the frequency and go into phase tracking mode. With the battery voltage increasing, the duty cycle decreases, i.e. I_b becomes pulsating and ultimately reaches to zero (i.e., charging is shut off) when the battery is fully charged. The complete charging process can be automatically implemented by using the inherent characteristics of CP-PLL by using popular ICs like 4046 or 9046.

The 3-state PFC discriminates between the leading and lagging phase unlike in normal PLL. In case of charging battery, current needs to be pumped into the battery and stopped when charging is complete. There is no need of withdrawing current to adjust leading phase. Thus output of the CP-PLL, in this case, should be either current pumping into the battery or high impedance state resulting in the desired current pulse train as I_b . Based upon the control

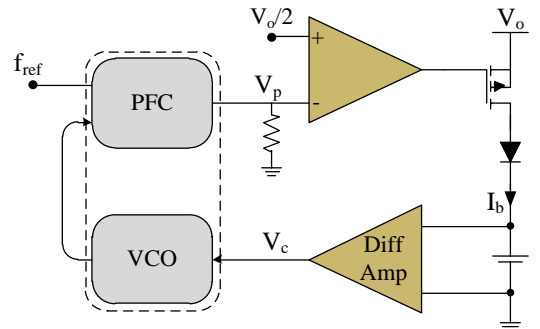


Figure 8: CPCB circuit overview [16]

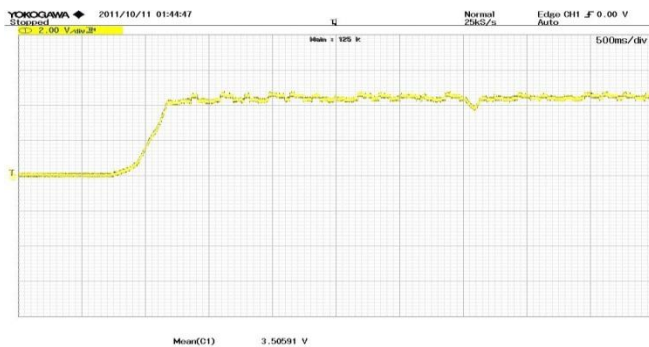


Figure 13: Actual voltage in secondary side [Experimental]

(set point tracking) can be seen in Figure 10 and Figure 12, where the reference voltage is initially set to 5 V, at $t=0.2$ s changed to 2 V, at $t=0.4$ s changed to 6 V and finally brought back to 5 V at $t=0.6$ s.

After verification with the simulation, a hardware prototype using discrete components was made. The test load was CPCB circuit with a rechargeable 300 mAh Li-Ion battery of 3.6 V. The actual voltage variation in the secondary side when mobile unit is brought from far away near to primary track and then slightly moved away is captured by Yokogawa DLM2022 Digital Storage Oscilloscope and shown in Figure 13. Further the error signal (green) and control action (yellow) with changing distance (in effect changing coupling) between primary and secondary side is depicted in Figure 14.

Practically it has been noticed that when the distance between primary and secondary coil is more than 26 mm the output voltage would drop below 4 V, and thus the pickup was unable to start under such a condition.

VII. CONCLUSION

An inductive power transfer scheme with primary controller, specially designed for biomedical implants, has been proposed and implemented successfully. It has been tested by charging a 3.6 V battery with satisfactory results. Authors proposed and validated that shifting the dissipative parts of power link to the primary side keeping minimal circuit in secondary helps prevent heating of the implant, also keeping minimal size. Additionally high efficiency battery charger has been used to minimize any heating of the battery during charging. Immediate future work is to fabricate an IC for secondary side and printed pickup coil. The proposed architecture can become a viable alternative to conventional powering schemes for biomedical implants and can be extended for general purpose contactless power transfer applications.

REFERENCES

[1] Yungtaek Jang; Jovanovic, M.M.; , "A contactless electrical energy transmission system for portable-telephone battery chargers," *Industrial Electronics, IEEE Transactions on* , vol.50, no.3, pp. 520-527, June 2003.

[2] Ping Si; Hu, A.P.; Malpas, S.; Budgett, D.; , "A Frequency Control Method for Regulating Wireless Power to Implantable Devices," *Biomedical Circuits and Systems, IEEE Transactions on* , vol.2, no.1, pp.22-29, March 2008.

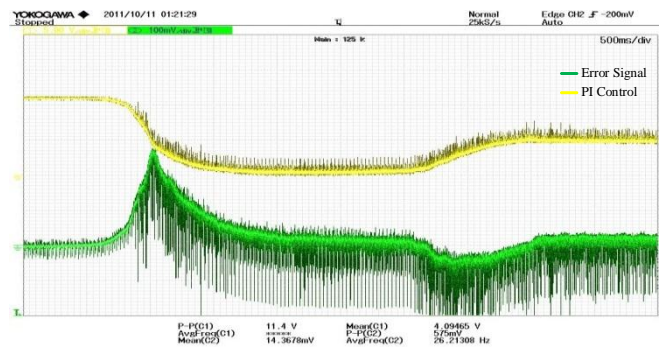


Figure 14: Error signal and PI Controller output [Experimental]

[3] Chwei-Sen Wang; Stielau, O.H.; Covic, G.A.; , "Design considerations for a contactless electric vehicle battery charger," *Industrial Electronics, IEEE Transactions on* , vol.52, no.5, pp. 1308-1314, Oct. 2005.

[4] Byungcho Choi; Jaehyun Nho; Honnyong Cha; Taeyoung Ahn; Seungwon Choi; , "Design and implementation of low-profile contactless battery charger using planar printed circuit board windings as energy transfer device," *Industrial Electronics, IEEE Transactions on* , vol.51, no.1, pp. 140- 147, Feb. 2004.

[5] Thrimawithana, D.J.; Madawala, U.K.; , "A primary side controller for inductive power transfer systems," *Industrial Technology (ICIT), 2010 IEEE International Conference on* , vol., no., pp.661-666, 14-17 March 2010.

[6] Zaheer, M.; Patel, N.; Hu, A.P.; , "Parallel tuned contactless power pickup using saturable core reactor," *Sustainable Energy Technologies (ICSET), 2010 IEEE International Conference on* , vol., no., pp.1-6, 6-9 Dec. 2010.

[7] Wu, H.H.; Boys, J.T.; Covic, G.A.; , "An AC Processing Pickup for IPT Systems," *Power Electronics, IEEE Transactions on* , vol.25, no.5, pp.1275-1284, May 2010.

[8] Keeling, N.A.; Covic, G.A.; Boys, J.T.; , "A Unity-Power-Factor IPT Pickup for High-Power Applications," *Industrial Electronics, IEEE Transactions on* , vol.57, no.2, pp.744-751, Feb. 2010.

[9] C. Strydis et al., "Implantable microelectronic devices: A comprehensive review," *Computer Engineering, TU Delft*, CE-TR-2006-01, Dec. 2006. Available: http://ce.et.tudelft.nl/publicationfiles/1038_555_thesis_strydis.pdf

[10] Dissanayake, Thushari D.; Budgett, David M.; Hu, Patrick; Bennet, Laura; Pyner, Susan; Booth, Lindsea; Amirapu, Satya; Wu, Yanzhen; Malpas, Simon C.; , "A Novel Low Temperature Transcutaneous Energy Transfer System Suitable for High Power Implantable Medical Devices: Performance and Validation in Sheep," *Artif. Organs*, vol. 34, no. Issue 5, pp. 160-167, May 2010.

[11] Puers, R.; Vandevoorde, G.; , "Recent progress on transcutaneous energy transfer for total artificial heart systems," *Artif. Organs*, vol. 25, no. Issue 5, pp. 400-405, May 2001.

[12] Guoxing Wang; Wentai Liu; Bashirullah, R.; Sivaprakasam, M.; Kendir, G.A.; Ying Ji; Humayun, M.S.; Weiland, J.D.; , "A closed loop transcutaneous power transfer system for implantable devices with enhanced stability," *Circuits and Systems, 2004. ISCAS '04. Proceedings of the 2004 International Symposium on*, vol.4, no., pp. IV- 17-20 Vol.4, 23-26 May 2004.

[13] Guoxing Wang; Wentai Liu; Sivaprakasam, M.; Kendir, G.A.; , "Design and analysis of an adaptive transcutaneous power telemetry for biomedical implants," *Circuits and Systems I: Regular Papers, IEEE Transactions on* , vol.52, no.10, pp. 2109- 2117, Oct. 2005.

[14] Artan, N.S.; Vanjani, H.; Vashist, G.; Zhen Fu; Bhakthavatsala, S.; Ludvig, N.; Medveczky, G.; Chao, H.J.; , "A high-performance transcutaneous battery charger for medical implants," *Engineering in Medicine and Biology Society (EMBC), 2010 Annual International Conference of the IEEE* , vol., no., pp.1581-1584, Aug. 31 2010-Sept. 4 2010.

[15] Shin-ichi Tobishima; Koji Takei; Yoji Sakurai; Jun-ichi Yamaki; , "Lithium ion cell safety," *Journal of Power Sources*, Volume 90, Issue 2, 1 October 2000, Pages 188-195.

[16] Liang-Rui Chen; Jin-Jia Chen; Neng-Yi Chu; Gia-Yo Han; , "Current-Pumped Battery Charger," *Industrial Electronics, IEEE Transactions on* , vol.55, no.6, pp.2482-2488, June 2008.